Med Bio Eng Comput (2007) 45:563–573
DOI 10.1007/s11517-007-0187-9

ORIGINAL ARTICLE

Risk factors for a pressure-related deep tissue injury: a theoretical model

Amit Gefen

Received: 14 December 2006 / Accepted: 4 April 2007 / Published online: 8 May 2007

Abstract Pressure-related deep tissue injury is the term recommended by the United States National Pressure Ulcer Advisory Panel to describe a potentially life-threatening form of pressure ulcers, characterized by the presence of necrotic tissue under intact skin, and associated with prolonged compression of muscle tissue under bony prominences. In this study, a theoretical model was used to determine the relative contributions of the backrest inclination angle during prolonged wheelchair sitting, the muscle tissue stiffness and curvature of the ischial tuberosities (ITs) to the risk for injury in the gluteus muscles that pad the IT bones during sitting. The model is based on Hertz's theory for analysis of contact pressures between a rigid half-sphere (bone) and an elastic half-space (muscle). Hertz's theory is coupled with an injury threshold and damage law for muscle—both obtained in previous studies in rats. The simulation outputs the time-dependent bone–muscle contact pressures and the injured area in the gluteus. We calculated the full-size (asymptotic) injured area in the gluteus and the time for injury onset for different sitting angles α((90–150°), muscle tissue long-term shear moduli G (250–1,200 Pa) and bone diameters D (8–18 mm). We then evaluated the sensitivity of model results to variations in these parameters, in order to determine how injury predictions are affected. In reclined sitting ($\alpha = 150°$) the full-size injured area was ~2.1-fold smaller and the time for injury onset was ~1.3-fold longer compared with erect sitting ($\alpha = 90°$). For greater G the full-size injured area was smaller but the time for injury onset was shorter, e.g., increasing G from 250 to 1200 Pa decreased the full-size injured area ~2.5-fold, but shortened the time for injury onset 6.2-fold. For smaller D the time for injury onset dropped, e.g., decreased ~1.5-fold when D decreased from 18 to 8 mm. Interestingly, the full-size injured area maximized at D of about 12 mm but decreased for smaller or larger D. The susceptibility to sitting-acquired deep tissue injury strongly depends on the geometrical and biomechanical characteristics of the bone–muscle interface, and, particularly, on the radius of curvature of the IT which mostly influenced the size of the wound, and on the muscle stiffness which dominantly affected the time for injury onset.

Keywords Pressure ulcer · Decubitus · Bedsore · Wheelchair sitting · Rehabilitation

1 Introduction

Permanent wheelchair sitting is nearly inevitable in patients with serious disorders of the central nervous system, e.g., spinal cord injury (SCI), progressive conditions of multiple sclerosis (MS) or amyotrophic lateral sclerosis (ALS, Lou Gehrig's disease), spina bifida, poliomyelitis, syringomyelia and others. Geriatric patients with muscular weakness may also spend most of their daytime while sitting. In these patients, sitting-acquired pressure ulcers are a major health-risk concern. Sitting-acquired pressure ulcers typically appear in soft tissues enveloping bony prominences that are compressed by the body-weight against the wheelchair's supporting surfaces (Fig. 1a). Most pressure ulcers that are associated with chronic sitting appear under the ischial tuberosities (IT), sacrum and coccyx [4, 20, 28, 29]. These ulcers may range in severity

A. Gefen (✉)
Department of Biomedical Engineering,
Faculty of Engineering, Tel Aviv University,
Tel Aviv 69978, Israel
e-mail: gefen@eng.tau.ac.il

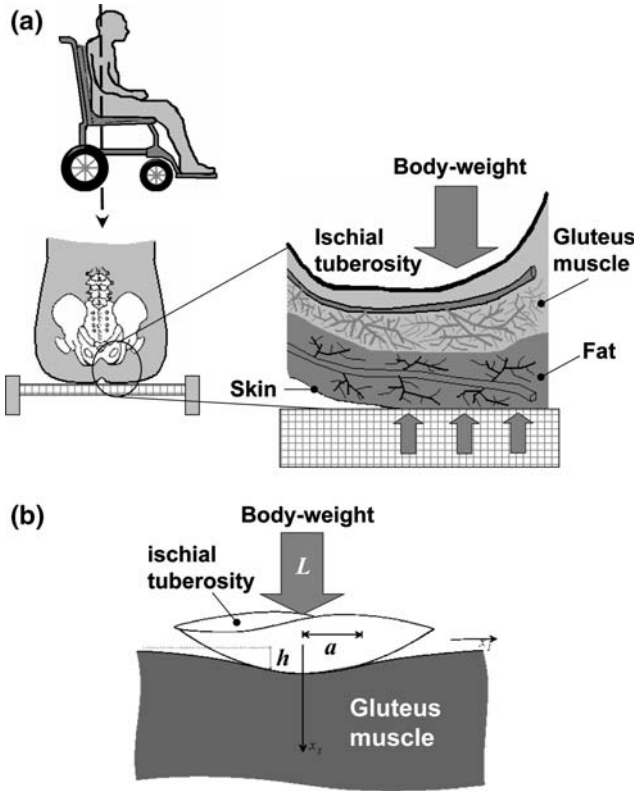

Fig. 1 The biomechanics of pressure-related deep tissue injury (DTI): **a** During immobilized wheelchair sitting, the *ischial tuberosity* (IT) continuously compresses the underlying soft tissue layers, whereas direct pressure is applied to the vascularized muscle tissue layer (*gluteus muscle*). For prolonged periods of continuous pressure, ischemic damage combined with excessive tissue deformation cause muscle tissue necrosis. (b) The theoretical model of DTI used herein employs the Hertz contact theory, and considers the IT as a *rigid half-sphere*, which compresses an *elastic half-space* which represents muscle tissue

from a superficial skin irritation to deep necrosis of muscle tissue [1, 5, 24].

In patients who suffer central nervous system disorders, the combination of immobilization of the lower extremities and buttocks during sitting, which imposes continuous, unrelieved internal soft tissue compression/shear stresses, with the lack or dysfunction of a pain ''alarm'' sensation, sets the conditions for local prolonged ischemia of vascularized tissues [11, 17]. Other than ischemia that leads to pressure necrosis, excessive prolonged soft tissue deformation due to the bone's compression was also indicated as causing cell death, which leads to pressure ulcers [6]. Mechanisms less understood than ischemia and tissue/cellular deformation, but which are believed to be involved in the onset of pressure ulcers include ischemia-reperfusion cycles, impaired metabolic activity and insufficient lymph drainage. Nevertheless, ischemia is traditionally considered to be the key factor in hypoxia-induced cell death that develops to a pressure ulcer [15]. Muscle tissue, the most vascularized tissue layer found between bone and skin during sitting, which is also the tissue with the highest metabolic demand, was reported to have the lowest tolerance to mechanical compression [8]. In other words, compression-induced pressure ulcers were shown to develop in muscle tissue of animal (pig) models at lower pressures, and faster than in fat or skin tissues [8].

Accordingly, in the recent years, it was recognized by the clinical as well as by the bioengineering communities that pressure ulcers can develop within muscle tissue which pads bony prominences, while, at the early stages of injury, there is no external indication that deep tissue necrosis has occurred [6, 11, 17, 25, 26]. The last (2005) Consensus Meeting of the US National Pressure Ulcer Advisory Panel (NPUAP) thereby introduced a new term, ''deep tissue injury'' (DTI), to classify injury cases belonging to this unique, potentially life-threatening form of pressure ulcers, which are characterized by the presence of necrotic tissue under intact skin [2, 5, 9, 23].

In this study, a theoretical, analytical model of the mechanical interaction between the IT bony prominence and the underlying gluteus muscle of a sitting person was developed. The model is based on Hertz's contact theory for analysis of contact pressures between a rigid half-sphere (IT bone) and an elastic half-space (gluteus muscle). Hertz's equations for the bone–muscle contact pressure distribution were coupled with experimental data from rat models of DTI which were obtained in previous studies: (i) a pressure-time injury threshold for muscle tissue [18] and (ii) a damage law for muscle tissue describing the muscle's time-dependent stiffening response under pressure [11]. The simulation outputs the time-dependent contact pressures in muscle at the bone–muscle interface, and the time-dependent injured muscle area. We calculated the full-size (asymptotic) injured area in the gluteus and the time for DTI onset, for different IT compression forces as related to the sitting posture (backrest angle of the wheelchair), as well as for different muscle tissue shear moduli and IT bone radii of curvature. We then evaluated the sensitivity of model results to variations in values of these parameters, in order to determine how the above parameters influence predictions of DTI onset time and severity.

Significantly, unlike previous finite element modeling studies of DTI in a chronic sitting posture, which required complex computations [6, 11], the present model relies on minimal, inexpensive computer power. This can be a major advantage for applications extending beyond basic research, for example, continuous, real-time model calculations to monitor the risk for DTI onset in individual patients.

2 Methods

2.1 Rationale for modeling

The pathomechanics of DTI is poorly understood, and risk factors specific to DTI (other than immobilization combined with neuropathy) were not yet characterized. It is difficult to conduct epidemiological studies in order to characterize the risk factors for DTI. First, in clinical cases, injury is usually not visible until serious tissue damage occurs [3], and by that time, the specific causes of the DTI may be masked by secondary complications, and can no longer be isolated. Another difficulty is that patient groups (SCI, MS, ALS, geriatric) and individual patients within a group are very distinct in functional capacities and pattern of daily activities. Animal studies are a reasonable alternative; however, it is difficult to reproduce the biomechanical bone–muscle interactions of human sitting in laboratory animals. Fortunately, biomechanical modeling of DTI formation during human sitting may overcome some of these difficulties. In particular, it permits the isolation of the individual factors in the bone–muscle mechanical interaction, and separation of contributions of structural anatomy characteristics from those of mechanical properties of tissues, to the overall risk for DTI. For example, we recently showed, using MRI measurements, that there exists a substantial variation in the radii of curvature of IT among healthy subjects (standard deviation over mean ~30%, [19]). Accordingly, from a biomechanical perspective, it can be claimed that individuals with small IT radii of curvature are more susceptible to DTI since their ''sharper'' bones produce higher stress concentrations in muscle tissue when being compressed against the gluteus muscles during sitting (Fig. 1a). This hypothesis, as well as the effect of gluteal muscle tissue stiffness—also showing substantial biological variability (~40%, [22]), and the effect of the sitting posture (manifested by the magnitude of force transferred through the IT) are investigated in the present modeling study.

2.2 Analysis of bone–muscle contact pressures

The theoretical model of DTI used herein employs the Hertz contact theory, and considers the IT bone as a rigid half-sphere with diameter D, which compresses an elastic half-space with shear modulus G that represents gluteus muscle tissue (Fig. 1b). The underlying assumptions of Hertz' theory, as related to the present IT-gluteus contact problem, are discussed in detail in Sect. 4.1.

The body-weight load transferred through the IT, L, causes an axisymmetric contact pressure distribution at the bone–muscle interface, $P(r)$, around the vertical central axis of the rigid half-sphere (marked as axis x_3 in Fig. 1b). The contact pressure distribution in this problem, $P(r)$, was solved by Lee and Radok [16]:

$$P(r) = P_0\sqrt{1 - r^2/a^2} \tag{1}$$

where r is the distance from the vertical central axis of the half-sphere (axis x_3 in Fig. 1b), a is the contact radius and P_0 is the peak contact pressure, which occurs at the point where the vertical central axis of the half-sphere crosses the contact region. The contact radius, a, depends on the (body–weight) load L, the half-sphere (IT bone) diameter D, and the mechanical properties of the elastic half-space (muscle)—i.e., its shear modulus G and Poisson's ratio v([16]:

$$a = \sqrt{[3]}\frac{3LD(1-v)}{16G} \tag{2}$$

The peak contact pressure is calculated from [16]:

$$P_0 = \frac{8}{\pi}\frac{G}{(1-v)}\frac{a}{D} = \left[\frac{96}{\pi^3}\left(\frac{G}{1-v}\right)^2\frac{L}{D^2}\right]^{1/3} \tag{3}$$

We previously measured radii of curvature of the human IT ($D/2$) in six healthy subjects (age 26–29 years, body-weight 55–90 kg) during sitting, by means of MRI scans taken at the anterior–posterior (A–P) plane in an open configuration [19]. We found that the radius of curvature of the IT in normals range between 7 and 15 mm, and the standard deviation from the mean radius of curvature was ~3 mm.However, as sharper tuberosities may bear a greater risk for DTI [19], and in lack of statistical data of IT radii of curvature from vulnerable populations, we decided to focus on the lower range of IT radius measurements. Hence, we considered radii of 4 to 9 mm in our present simulations, so that the sharpest IT considered in our simulations represented one standard deviation below the radius of the IT of our (healthy) subject with the sharpest IT [19].

Since in vivo, muscle tissue contains mostly water (~75% of wet weight), it can be considered (nearly) incompressible, i.e., its Poisson's ratio can be taken as v = 0.5. Considering that DTI occurs over timescales of minutes to hours, but viscoelastic stress relaxation of fresh muscle tissue in the transverse direction (i.e., when being compressed by bone perpendicularly to the direction of muscle fibers, as in sitting) occurs within ~20 s [22], we considered G as the long-term shear modulus of muscle tissue. Values of long-term G in the transverse direction of muscle, 250–1,200 Pa, were measured in a previous study in fresh porcine gluteal muscles subjected to large deformations [22].

For the purpose of modeling we assumed that during static sitting, the two ITs transfer equal loads to the underlying soft tissues. Accordingly, the load L transferred to gluteal muscle tissue during static sitting through one IT is calculated from:

$$L = \frac{\phi \cdot \mathrm{BM} \cdot g}{2} \sin(180^\circ - \alpha) \tag{4}$$

where $\phi = 0.686$ is the weight fraction of the upper body including the head, neck and trunk [30], BM is the person's body mass (in kg), g is the acceleration of gravity 9.81 m/s^2) and $\alpha(^\circ)$ is the angle of the wheelchair's backrest [17]. A body mass of BM = 70 kg was set in all simulations. Wheelchair backrest angles of 90° (erect sitting) to 150° (reclined sitting) were considered.

Overall, for a subject with body mass BM, wheelchair backrest inclination α, IT bone radius $D/2$, and shear modulus of (incompressible) muscle tissue G, Eqs. (1)–(4) are employed to calculate the axisymmetric distribution of bone–muscle contact pressures between the IT and gluteus, $P(r)$.

2.3 Pressure-time injury threshold for muscle tissue

Critical magnitudes of bone–muscle contact pressure distributions $P(r)$ or critical time exposures to $P(r)$ values (exceeding the tissue's injury threshold) can induce muscle cell death [18]. Accordingly, a pressure–time injury threshold for muscle tissue was coupled into the simulations to predict the extent of injury caused by continuous, unrelieved exposures to $P(r)$ for a subject with body characteristics BM and $D/2$, muscle tissue stiffness G and wheelchair backrest position α. We employed our previously published cell death threshold for skeletal muscle tissue of rats [18] which is based on muscle tissue compression experiments followed by histology in 174 mature albino rat models of DTI. As described in detail in [18], the pressure-time function which best distinguished all muscle injury cases from non-injury cases, where muscle injury was defined as either the occurrence of muscle cell death or the loss of the tissue's cross-striation architecture was:

$$P_{[\mathrm{kPa}]} = \frac{K}{1 + e^{\lambda(t - t_0)}} + C \tag{5}$$

where the constants of the pressure–time injury threshold are K =23 kPa, $\lambda = 0.15$ min^{-1}, $t_0 = 95$ min, and C = 8kPa.

2.4 Stiffening response of injured muscle tissue

Simulations of DTI need to take the altered mechanical behavior of injured muscle tissue into account, as the altered mechanical properties of injured muscle tissue may affect mechanical stresses in adjacent, normal tissues [11, 17]. Using indentation testing of gracilis muscles of albino rat DTI models (in a group of 42 animals) we previously found that muscle tissue, which is subjected to prolonged pressure stiffens post-injury [11]. We also found that the extent of stiffening post-injury is proportional to the magnitude of the applied pressure P as well as to the exposure time t. The methodology and results of these animal studies are described in details in [11]. In brief, we found that the ratio of the long-term shear modulus of muscle tissue post-injury over its baseline (pre-injury) shear modulus, $\bar{G}_{\mathrm{injury}}$, can be described using multiple linear regression as a linear function of P and t [11]:

$$\bar{G}_{\mathrm{injury}} = A_0 + A_1 P + A_2 t \tag{6}$$

where the constants are $A_0 = 0.25$, $A_1 = 0.022$ kPa^{-1}, $A_2 = 0.0125$ min^{-1}, $P \leq 70$ kPa, and $t \leq 120$ min. Values of the dimensionless property ratio $\bar{G}_{\mathrm{injury}}$ range from 1.2 for minimal pressure exposures (P = 35 kPa for t = 15 min) to 3.3 for maximal pressure exposures (P=70 kPa for 120 min). Analysis of variance and subsequent t-tests for the coefficients A_1, A_2 confirmed that fitting the linear Eq. (6) to our experimental data from rat gracilis muscles was adequate, and the mean predictive error of Eq. (6) with respect to raw $\bar{G}_{\mathrm{injury}}$ experimental data (Table 3 in [11]) was calculated to be 3%. Eq. (6) was therefore employed in the present model to determine the extent of stiffening of muscle tissue, which has been identified by Eq. (5) as injured.

2.5 Algorithm and protocol of computer simulations

The animal studies reviewed in Sects. 2.3 and 2.4 [11, 17, 18] demonstrated that bone–muscle contact pressures, which exceed a critical level and duration, not only induce muscle cell death but also cause abnormal stiffening of the muscle tissue. It has been suggested that this rise in tissue stiffness is caused by cellular decomposition resulting in the rise in the swelling pressure of the tissue, or by intracellular proteolysis, or by local ''rigor mortis'' in muscle tissue [17]. Consequent to the stiffening of muscle tissue with the onset of DTI, the distribution of mechanical stresses around the bone–muscle interface changes, and stresses increase in magnitude and expand over wider tissue regions [11, 17]. This essentially exposes additional uninjured regions of muscle tissue (or adjacent tissues) to intensified stresses [11, 17]. The spreading increase in muscle tissue stresses may cause additional obstructions or occlusions of capillaries in addition to the mechanical conditions already imposed by

the immobilized sitting, and thereby, tissue regions that are affected by ischemia and hypoxia are likely to widen. Eventually, additional muscle cell death occurs, which then triggers additional muscle tissue stiffening in an ongoing, positive-feedback injury spiral [11]. A computer model, employing engineering quantitative characterizations of these processes—in the form of Eqs. (1)–(6)—was developed to simulate this pressure-injury-stiffening spiral in DTI progression, and to identify the potential roles of some anatomical and tissue mechanical characteristics in DTI progression, as follows.

The algorithm, implemented using a Matlab 7 software code (MathWorks Co.) is described in the flowchart given in Fig. 2. Inputs to the DTI model are the body mass BM, the IT radius of curvature $D/2$, and the long-term shear modulus of gluteus muscle tissue G. Using the Hertz contact theory Eqs. (1)–(3), the algorithm calculates the bone–muscle pressure distribution $P(r)$ occurring as a result of an IT load L associated with a wheelchair's backrest angle α [Eq. (4)]. A time-step increase of $\Delta t = 6$ min is assumed. Following each Δt it is checked whether $P(r)$ applied during the accumulative exposure time t exceeds the muscle injury threshold in Eq. (5). If injury is detected, the algorithm calculates the area of predicted DTI, i.e., the radius at which muscle pressures $P(r)$ exceed the injury threshold of Eq. (5). If the calculated injured muscle area is similar to that calculated in the previous iteration—within less than 0.01 cm^2 difference—a ''steady state'' of the DTI is assumed, and the simulation terminates. If, however, the difference between injured areas across subsequent simulation steps exceeds 0.01 cm^2, the effect of injury on the shear modulus of muscle tissue G is taken into account, by multiplying G by the property ratio $\bar{G}_{\text{injury}}$ [Eq. (6)]. The algorithm then recalculates $P(r)$ using Eqs. (1)–(3) owing to the increase in the injured muscle's shear modulus by a factor of $\bar{G}_{\text{injury}}$. Next, the time step increases by Δt again, and the new $P(r)$ is compared with the muscle's injury threshold in Eq. (5). This iterative process repeats until the simulation converges to a steady injured muscle area—the full-size injury.

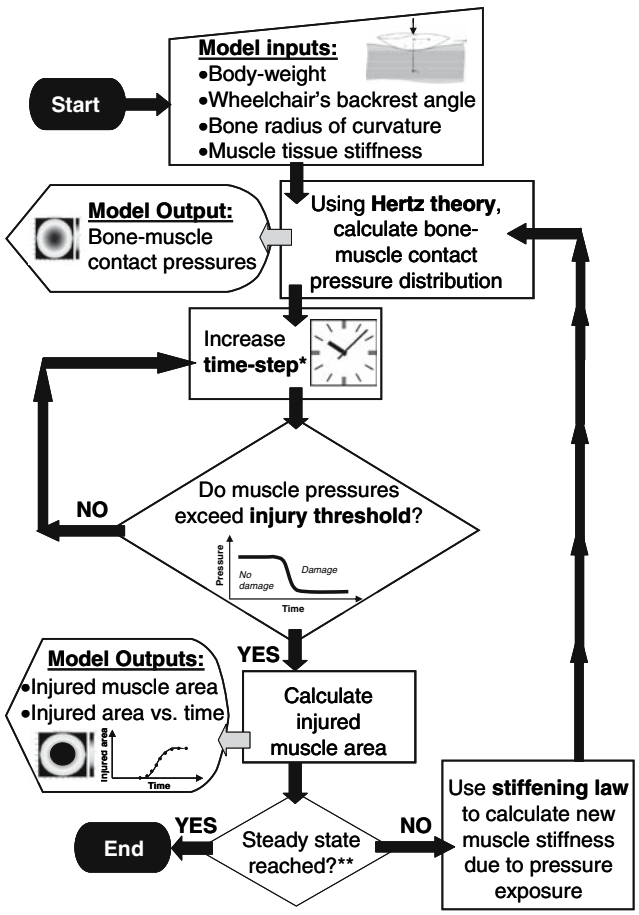

Fig. 2 Flowchart of the simulation process. *Asterisk* represents time-step increases are at 6 min intervals. *Double asterisk* represents steady state is assumed when changes in the injured area between subsequent simulation iterations are less than 0.01 cm^2

In preliminary analyses, we determined the sensitivity of model predictions (DTI onset time, full-size injured area) to changes in the selected time step Δt, and found that results were invariant to Δt as long as the selected Δt was set as being shorter than half the shortest duration for which experimental data of pressure–time injury threshold exists (that is, 15 min in [18]), i.e., we required that $\Delta t < 7.5$ min. Accordingly, $\Delta t = 6$ min was selected for computational efficiency. Normally, our simulations required several seconds to run the iterative calculations described in Fig. 2, and convergence to a full-size injured muscle area was evident in all simulations after less than 25 iteration steps (for $\Delta t = 6$ min).

In order to determine the effects of model input parameters of the wheelchair's backrest inclination α, the IT radius of curvature $D/2$ and the muscle's (uninjured) shear modulus G on the full-size of the injured muscle area and the time for onset of DTI, we ran 20 simulation cases, changing one input parameter each time and keeping all other at reference values (as detailed in Table 1). The ±40% variations in the gluteus muscle's long-term shear modulus G and the IT's radius of curvature $D/2$ (Table 1) represent biological variability of measured data, in [22] and [19], respectively. For each simulation case, we plotted the bone–muscle contact pressure distribution $P(r)$ at discrete time steps Δt, and, if applicable, we superimposed the predicted injured muscle area versus time on the $P(r)$ versus t plots. Last, we determined the time for onset of DTI and the full-size of the injured muscle area, from each plot of injured muscle area versus time.

Table 1 Sensitivity of the deep tissue injury (DTI) model predictions to variations in model parameter values

Parameter (reference value of each parameter is provided in parentheses)	Variation (%)	Effect (%)	
		Asymptotic injured muscle area	Time to DTI onset
Backrest angle (α = 90°)	+40	–11	+10
Gluteus muscle's long-term shear modulus[a]	+40	–10	–38
G = 725 Pa	–40	+39	+163
Ischial tuberosity's radius of curvature[b]	+40	–88	+14
$D/2$ = 6.5 mm	–40	–19	–25

Variations in the gluteus muscle's long-term shear modulus and the ischial tuberosity's radius of curvature represent biological variability of measured data, in [22] and [19], respectively

[a] Measured in fresh porcine gluteus muscles (adapted from [22])

[b] Measured by means of MRI scans of sitting (healthy) subjects (adapted from [19])

3 Results

We tested the effects of variations in model input parameters (the wheelchair's backrest angle α, the gluteus muscle's long-term shear modulus G, and the IT radius of curvature $D/2$) on the predicted full-size (asymptotic) injured muscle area, and on the time for DTI onset (Table 1). An example of model-predicted time-dependent bone–muscle contact pressure distributions $P(r)$ and corresponding injured muscle areas is depicted in Fig. 3, and plots of injured muscle area versus time for all simulation cases are provided in Fig. 4.

Variations of the wheelchair's backrest angle α in the range of 90–150°, the long-term shear modulus of the gluteus muscle G in the range of ±40%, and the IT radius of curvature $D/2$, also in the range of ±40%, caused substantial variations in model predictions of the full-size injured muscle area, and the time for DTI onset. Specifically, full-size injured muscle areas varied between 14 and 130 cm^2 and DTI onset times varied between 15 and 123 min for the above range of variations in input parameters α, G and $D/2$.

The results shown in Fig. 4a revealed that for larger wheelchair's backrest angles, the predicted asymptotic injured muscle area tended to decrease and the time for DTI onset increased (Table 1). For example, the model predicted that during immobilized reclined sitting with a backrest inclination of 150°, DTI onset occurs after 111 min and the full-size DTI eventually covers a muscle area of 53 cm^2. In contrast, during erect (90°) sitting of the same subject (i.e., with same IT radius $D/2$ = 6.5 mm and muscle tissue shear modulus G = 725 Pa), a DTI onsets as early as 87 min after immobilized sitting, and the full-size wound is expected to occupy 110 cm^2 of muscle tissue under the IT (Fig. 4a). Generally, for sitting at $\alpha \leq 120°$ there is very little effect of increasing the wheelchair's backrest angle on the asymptotic injured muscle area (maximum 8%), and, there is no effect on the time for DTI onset. However, in reclined postures, i.e., for $\alpha \geq 130°$, there is more substantial decrease in the full-size of the injured area and the DTI onset time rises (Fig. 4a).

For greater muscle tissue long-term shear modulus values (G) the full-size injured muscle areas were smaller, but the time for onset of DTI was shorter (Fig. 4b, Table 1). For example, increasing G from 250 to 1,200 Pa decreased the predicted full-size DTI area ~2.5-fold, but shortened the time for injury onset 6.2-fold (Fig. 4b). Again, the effect of muscle stiffness was highly non-linear (Fig. 4b), with variations of G in the lower domain (250–550 Pa) having a more substantial effect on the full-size injured area and DTI onset time, with respect to G variations in the higher domain (850–1,200 Pa).

For smaller IT bone radii the time for injury was found to be shorter (e.g., decreased ~1.5-fold when radii decrease from 9 to 4 mm), and the predicted full-size injured area maximized at IT radii of around 6 mm (~130 cm^2), but decreased for smaller or larger IT radii.

Taken together, the simulation results indicated that the susceptibility to sitting-acquired DTI and the severity of wounds strongly depend on the geometrical and biomechanical characteristics of the bone–muscle interface and particularly, on the IT radius of curvature which mostly influenced the size of the injured area (Fig. 4c, Table 1), and on the muscle stiffness (shear modulus) which dominantly affected the time for DTI onset (Fig. 4b, Table 1).

4 Discussion

Following its 2005 Consensus Meeting, the NPUAP strongly encourages investigators to study the etiology and epidemiology of pressure-related DTI, since it was recognized in that meeting that DTI are very likely to develop to life-threatening full-thickness pressure ulcers even with treatment [2]. In particular, it is still unknown to what extent does the sitting posture affect the risk for DTI development, and also, whether certain anatomical structures of the pelvis or mechanical properties of the buttocks' tissues increase the susceptibility to DTI. The present model of DTI progression in the gluteus muscle under the IT was developed as a first step toward determining these effects. We found that the sitting posture, the stiffness of muscle tissue and the sharpness of the IT—all have substantial influence on the DTI onset time and the extent of muscle tissue damage (Fig. 4).

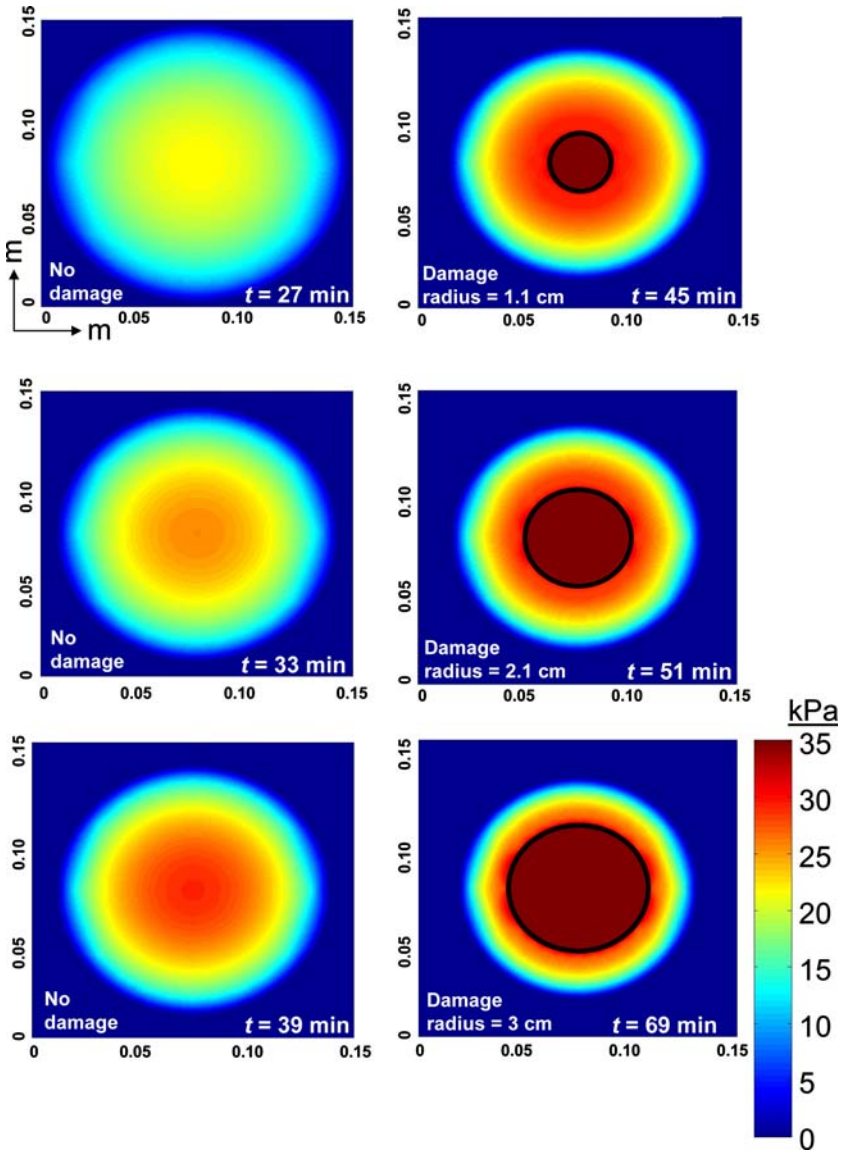

Fig. 3 Model predicted time-dependent distributions of contact pressures between the ischial tuberosity (IT) and gluteal muscle, for a simulation case considering body-weight of 70 kg, erect wheelchair sitting (90° backrest angle), IT radius of curvature of 5 mm, and (uninjured) gluteal muscle shear modulus of 500 Pa. For this simulation case, injury onsets between the 39 and 45 min simulation frames, and the time-dependent injured area is depicted over the stress distribution plots as *brown circles* with *black margins*

Interestingly, the model indications that larger wheelchair backrest angles delay the onset of DTI and reduce the injured muscle area if injury onsets (Fig. 4a, Table 1) support classic medical protocols for pressure ulcer prevention among wheelchair-bound individuals, e.g., Griffith's protocol which recommends 15 min of lying following every 2 h of sitting [13].

The time for DTI onset, in particular, was shown to vary considerably across simulation cases, from 15 min to approximately 2 h (Fig. 4). This is relevant in regard to development of pressure-relieving programs for wheelchair-bound patients. Currently, US and European health services advise body-able wheelchair users to perform a pressure-relieving movement every 15 min [14, 27]. However, many wheelchair users report that they do not follow these recommendations, e.g., one survey found that ~21% of patients moved only once an hour and further ~55% moved less often than once an hour [27]. The results of the present simulations indicate a likelihood that not all patients need to perform pressure-relieving maneuvers every 15 min, as patients with less sharp ITs and less stiff muscle tissue may be more protected inherently. Therefore, with the aid of biomechanical modeling of DTI, preventative health behaviors of chronic wheelchair users may be tailor-made, based on their natural sitting posture, anatomical characteristics and the biomechanical properties of their tissues.

4.1 Assumptions of Hertz's theory and related limitations of the model

The model used in this paper is based on Hertz's contact theory, which is employed to describe the bone–muscle mechanical interaction. The Hertz contact theory involves

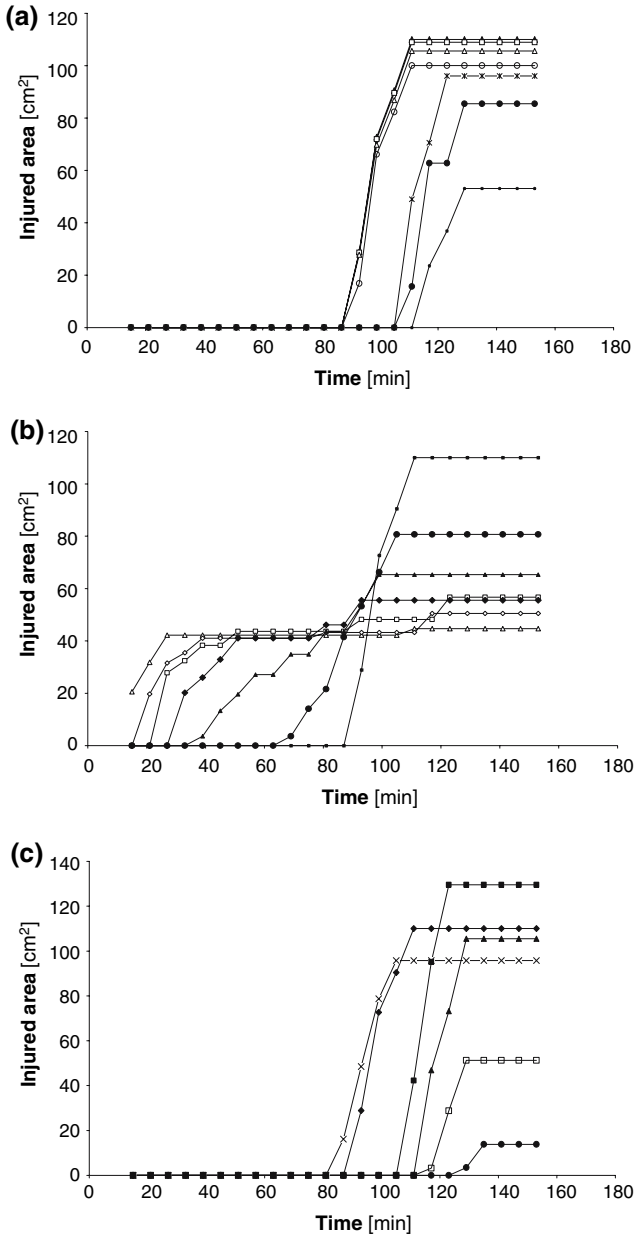

Fig. 4 Effect of model parameters on the predictions of time for injury onset and size of the injured area. **a** The injured area versus time for different values of the wheelchair's backrest angle: (*dark filled triangle*) 90°; (*open square*) 100°; (*open triangle*) 110°; (*open circle*) 120°; (— ?—) 130°; (*dark filled circle*) 140°; (*dark filled square*) 150°. **b** The injured area versus time for different values of long-term shear modulus of muscle tissue: (*dark filled square*) 250 Pa; (*dark filled circle*) 400 Pa; (*dark filled triangle*) 550 Pa; (*dark filled diamond*) 700 Pa; (*open square*) 850 Pa; (*open diamond*) 1,000 Pa; (*open triangle*) 1,200 Pa. **c** The injured area versus time for different values of the ischial tuberosity's radius of curvature: (—×—) 4 mm; (*dark filled diamond*) 5 mm; (*dark filled square*) 6 mm; (*dark filled triangle*) 7 mm; (*open square*) 8 mm; (*dark filled circle*) 9 mm

several underlying assumptions, as follows [10]: (1) The two contacting bodies are homogenous, isotropic and linear elastic (or one body is linear elastic and the other is rigid, as herein). (2) The dimensions of each body are large compared with the radius of the circle of contact. (3) All deformations occur in the elastic range. (4) The contacting bodies are in frictionless contact, that is, only a normal stress (pressure) is transmitted via the contact interface.

One of the most well known scenarios for utilization of Hertz's theory is the contact between a rigid half-sphere and a flat semi-infinite surface [16] which are considered herein to represent the IT bone and gluteus muscle, respectively. This allowed analytical investigation of DTI onset and progression with a small set of model parameters, which is an essential first step toward more advanced DTI modeling, because the dominant biomechanical factors that are involved may be identified and their role be characterized in a relatively easy, straightforward manner. However, in reality, the IT is not a perfect half-sphere: in MRI scans taken at the A–P plane its profile appears to be somewhat elliptical [19], which probably induces higher peak contact stresses on the gluteus than those predictable by a half-sphere model, owing to the ''sharper'' true bone shape. Likewise, the gluteus is not flat (it is actually covering the bone during sitting [19], nor is it large enough to satisfy Hertz's semi-infinite boundary conditions. We also assumed, in lack of experimental data in the literature, that the geometry of the IT that is in contact with the gluteus is the same in the range of body postures investigated herein (sitting erect to reclined), while in reality, this geometry may be posture-dependent. Hence, certain errors, which relate to the non-ideal geometry are introduced into the model predictions. Other than errors associated with the compromised geometry, there are also inaccuracies due to the large deformations in muscle tissue adjacent to the IT during sitting [19] which were not considered in the original theory of Hertz. Last, in reality, the contact between the bone and muscle is not perfectly smooth, and shear stresses associated with friction may develop at the bone–muscle interface while sitting [19]. In order to obtain first approximations of the errors in model predictions caused by these inconsistencies with respect to the original Hertz assumptions, we followed the work of Zheng and colleagues [7, 31, 32]. These authors conducted comprehensive experimental and computational (finite element) studies of the effects of factors involved in the ''real-world'' situation, i.e., compromised geometry, large deformations and friction, on the accuracy of solutions of a similar Hertzian problem, of a cylindrical flat-ended rigid body compressing an elastic half-space.

The extent of compromise in a problem's geometry with respect to the Hertzian assumption is evaluated by means of the aspect ratio: the radius of the indenting rigid body over the thickness of the (undeformed) indented elastic body. Ideally, for a half-space with infinite thickness, the aspect ratio equals 0, and it rises above 0 for all (realistic)

problems with finite dimensions. By means of MRI (in the A–P plane), we previously found that in six subjects the radius of curvature of the IT, $D/2$, ranged between 7 and 15 mm (mean 12 mm) and the thickness of the undeformed gluteus muscle under the IT, T, ranged between 17 and 27 mm (mean 21 mm) [19]. Accordingly, the aspect ratio $0.5D/T$ for the IT-gluteus contact problem ranges between 0.37 and 0.79 (mean 0.6) [19].

In vitro experiments on fresh fish tissue layers demonstrated that contact problems with aspect ratios $0.5D/T < 0.25$ produce negligible errors when Hertz's theory is used to determine the elastic properties of the indented body, or the contact pressures on the indented body [32]. A later study determined the combined effect of larger aspect ratios and large deformations on Hertz's theory, by means of finite element analyses [7]. These authors found that under such circumstances, errors of the Hertz equations were under 15% as long as the aspect ratio $0.5D/T$ was smaller than 1 [7]. With respect to the influence of ignoring the friction at the bone–muscle interface, it was found that for an aspect ratio of 0.6, as in the present application, the difference between results obtained while considering large deformation contacts with or without friction at the interface was only 2% [31]. Taking these studies together, we conclude that the dominant source of error associated with application of Hertz's contact theory to the investigation of the IT-gluteus mechanical interaction is the combined effect of relatively large aspect ratio with large deformations (error ~15%, [7]). The effect of not considering friction, however, is much less (additional error of 2%, [31]). Overall, for the present first modeling attempt to describe the factors that potentially determine the susceptibility to DTI, such errors are reasonable, particularly when considering possible effects of other sources of uncertainty such as the biological variability in the muscle's shear modulus G, for which approximations may be subjected to imprecision of ~40% [22].

Despite the observation that frictional shear stresses have minor mechanical influence on the effective contact stresses for the aspect ratio relevant to the IT-gluteus contact problem represented by Hertz's theory (2% according to [31]), their biological effect on muscle tissue viability for even low shear stress values can be substantial [21]. Specifically, shear stresses can cause changes in the angles of the muscle's blood vessels, and thus, they add to the effect of compression in obstructing or occluding blood supply, which results in more ischemia, cellular death, and tissue necrosis [21]. Unfortunately, an injury threshold for muscle tissue subjected to shear stress, analogous to the injury threshold for muscle tissue under compression which was used herein [Eq. (5), [18]], is still missing in the literature, and so, this topic warrants further investigations.

One last model assumption that is left to discuss is embedded in Eq. (6), which considers stiffening of the whole muscle if an injury onsets, whereas in reality, the damage (and stiffening) starts locally around the bone–muscle interface [11, 17]. This assumption was taken because Hertz's theory requires the indented body to be considered as a homogenous material, and so, local increases in muscle stiffness were not possible by means of the present model. Accordingly, the present model is also not suitable for considering widening of a DTI into deep muscle layers that are distal from the IT, because it cannot treat stress distributions within internal muscle tissue regions having different mechanical properties—a task which requires numerical (e.g., finite element) methods [11, 17]. However, on a retrospect, it appears that this assumption had little effect on the model results. First and foremost, there is no effect at all on the predictions of times for DTI onset, since these predictions depend only on the initial (non-injured condition) calculation of IT-gluteus contact pressures and on the injury threshold (Fig. 2). The rates of injury progression (once started) and the full-size injured areas—while being consistent in trend with our previous numerical studies [11, 17]—are likely to be overestimated by the present model because contact stresses herein should be generally higher than for a case of local tissue stiffening (where uninjured parts of the muscle remain at lower stiffness). Yet, despite being overestimated in size, all simulated injuries were still contained in the relatively small anatomical region of the bone–muscle contact site: the maximal ratio of radii of the full-size injured area over the IT-gluteus contact area was 1.45, across all simulation cases. Accordingly, the overestimation bias associated with the formulation of Eq. (6) has little practical importance for interpretation of the findings.

4.2 Closing comments

The analytical DTI model presented in this paper offers several advantages, and has several limitations, with respect to previous numerical (finite element) models of DTI [11, 17]. On the advantage side, the small set of parameters in the present model allows to determine the separate effects of IT sharpness and gluteal stiffness in a straightforward, elegant manner, which promotes understanding of the etiology of DTI. On the disadvantage side, the simplified geometrical representation of the bone–muscle contact surfaces, and likewise, the simple constitutive law used herein, make the present results indicative, more than definitive. In other words, while the trends of effects of model parameters are well demonstrated by means of Eqs. (1)–(6), ''real-world'' bone–muscle biomechanical interactions as related to DTI are more complex (as discussed in detail in Sect. 4.1 above),

and are affected by factors such as large muscle tissue deformations and strains, geometrical irregularities of the bone surface, no homogeneity of muscle tissue and quality of the local blood perfusion in muscle tissue. Another reservation is that the injury threshold [Eq. (5)] and damage law [Eq. (6)] used herein for muscle tissue are adopted from rat models of DTI [11, 18], and their applicability to human DTI cannot be fully determined. Though injury thresholds for human muscle tissue under compression are not yet available, tissue-engineering work may, in the future, allow the acquisition of such data from bioartificial muscles formed in vitro, from human cells [6]. The present model can then be refined to rely on the human-based experimental data.

With that being said, we found that the IT radius of curvature mostly influenced the size of the injured area, and muscle stiffness strongly affected the time for DTI onset (Fig. 4b, c). These results indicate that there appear to be two important risk factors (other than just immobilization and neuropathy) for DTI, namely, a sharp IT shape and a stiff gluteus tissue, which are presently overlooked, but can be identified rather easily in the clinical setting. For example, an ultrasound scan of the buttocks can determine the radius of curvature of the IT, and, if coupled with elastography [12], it can also evaluate the shear modulus of the glutei. Yet, it should be appreciated that due to the simplifications made in the present model, further research employing more advanced models will be required before any practical or clinical implications can be derived. Accordingly, patient studies are currently underway in our laboratory, using the methodology described in [19], to gain experimental evidences that wheelchair-bound individuals having one or two of the above-mentioned risk factors are indeed more susceptible to DTI.

Acknowledgments My students Ms Ayelet Glass and Mr Eran Atlas are thanked for running the Matlab simulations. This study was partially supported by research grants from the Israeli Association for the Study of Diabetes, from the Chief Scientist's Office of the Ministry of Health, Israel, and from the Nicholas and Elizabeth Slezak Super Center for Cardiac Research and Biomedical Engineering.

References

1. Agency for Health Care Policy and Research (AHCPR) (1994) Treatment of pressure ulcers. Clinical practice guideline no. 15. Publication no. 95-0652. US Department of Health and Human Services, Rockville
2. Ankrom MA, Bennett RG, Sprigle S, Langemo D, Black JM, Berlowitz DR, Lyder CH, National Pressure Ulcer Advisory Panel (2005) Pressure-related deep tissue injury under intact skin and the current pressure ulcer staging systems. Adv Skin Wound Care 18:35–42
3. Bansal C, Scott R, Stewart D, Cockerell CJ (2005) Decubitus ulcers: a review of the literature. Int J Dermatol 44:805–810
4. Barbenel J (1984) The prevalence of pressure sores. National symposium on the care, treatment, and prevention of decubitus ulcers. Conference proceedings, 1–9
5. Black JM (2005) National Pressure Ulcer Advisory Panel. Moving toward consensus on deep tissue injury and pressure ulcer staging. Adv Skin Wound Care 18:415–421
6. Bouten CV, Oomens CW, Baaijens FP, Bader DL (2003) The etiology of pressure ulcers: skin deep or muscle bound? Arch Phys Med Rehabil 84:616–619
7. Choi APC, Zheng YP (2005) Estimation of Young's modulus and Poisson's ratio of soft tissue from indentation using two different-sized indentors: finite element analysis of the finite deformation effect. Med Biol Eng Comput 43:258–264
8. Daniel RK, Priest DL, Wheatley DC (1981) Etiologic factors in pressure sores: an experimental model. Arch Phys Med Rehabil 62:492–498
9. Doughty D, Ramundom J, Bonham P, Beitz J, Erwin-Toth P, Anderson R, Rolstad BS (2006) Issues and challenges in staging of pressure ulcers. J Wound Ostomy Continence Nurs 33:125–130
10. Fischer-Cripps AC (1999) The Hertzian contact surface. J Mater Sci 34:129–137
11. Gefen A, Gefen N, Linder-Ganz E, Margulies SS (2005). In vivo muscle stiffening under bone compression promotes deep pressure sores. J Biomech Eng 127:512–524
12. Gennisson JL, Cornu C, Catheline S, Fink M, Portero P (2005) Human muscle hardness assessment during incremental isometric contraction using transient elastography. J Biomech 38: 1543–1550
13. Griffith BH (1963) Advances in the treatment of decubitus ulcers. Surg Clin North Am 43:245–260
14. Hess CT (2004) Care tips for chronic wounds: pressure ulcers. Adv Skin Wound Care 17:477–479
15. Kosiak M (1961) Etiology of decubitus ulcers. Arch Phys Med Rehabil 42:19–29
16. Lee EH, Radok JRM (1960) The contact problem for viscoelastic bodies. J Appl Mech 27E: 438–444
17. Linder-Ganz E, Gefen A (2004) Mechanical compression-induced pressure sores in rat hindlimb: muscle stiffness, histology, and computational models. J Appl Physiol 96:2034–2049
18. Linder-Ganz E, Engelberg S, Scheinowitz M, Gefen A (2006) Pressure-time cell death threshold for albino rat skeletal muscles as related to pressure sore biomechanics. J Biomech 39:2725–2732
19. Linder-Ganz E, Shabshin N, Itzchak Y, Gefen A (2007) Assessment of mechanical conditions in sub-dermal tissues during sitting: a combined experimental-MRI and finite element approach. J Biomech 40:1443–1454. doi:10.1016/j.jbiomech.2006.06.020
20. Meehan M (1994) National pressure ulcer prevalence survey. Adv Wound Care 7:27–37
21. Niezgoda JA, Mendez-Eastman S (2006) The effective management of pressure ulcers. Adv Skin Wound Care 19(Suppl):3–15
22. Palevski A, Glaich I, Portnoy S, Linder-Ganz E, Gefen A (2006) Stress relaxation of porcine gluteus muscle subjected to sudden transverse deformation as related to pressure sore modeling. J Biomech Eng 128:782–787
23. Salcido R (2006) What is the ''purple heel''? Adv Skin Wound Care 19:11
24. Shea JD (1975) Pressure sores: classification and management. Clin Orthop 112:89–100
25. Stekelenburg A, Oomens CW, Strijkers GJ, de Graaf L, Bader DL, Nicolay K. (2006) A new MR-compatible loading device to study in vivo muscle damage development in rats due to compressive loading. Med Eng Phys 28:331–338
26. Stekelenburg A, Oomens CW, Strijkers GJ, Nicolay K, Bader DL (2006) Compression-induced deep tissue injury examined with

magnetic resonance imaging and histology. J Appl Physiol 100: 1946–1954
27. Stockton L, Parker D (2002) Pressure relief behaviour and the prevention of pressure ulcers in wheelchair users in the community. J Tissue Viability 12:84–92
28. Thomas DR (2001) Prevention and treatment of pressure ulcers. What works? What doesn't? Cleve Clin J Med 68:704–722
29. Vasconez LO, Schneider WJ, Jurkiewicz MJ (1977) Pressure sores. Curr Prob Surg 62:1–62
30. Winter DA (1990) Biomechanics and motor control of human movement, 2nd edn. Wiley, New York
31. Zheng M, Zheng YP, Mak AFT (1997) Estimating the effective Young's modulus of soft tissues from indentation tests—nonlinear finite element analysis of effects of friction and large deformation. Med Eng Phys 19:512–517
32. Zheng Y, Mak AF, Lue B (1999) Objective assessment of limb tissue elasticity: development of a manual indentation procedure. J Rehabil Res Dev 36:71–85